

## **A numerical study of time-dependent Schrödinger equation for multiphoton vibrational interaction of NO molecule, modelled as Morse oscillator, with intense far-infrared femtosecond lasers<sup>†</sup>**

AMITA WADEHRA and B M DEB\*<sup>#</sup>

Theoretical Chemistry Group, Department of Chemistry, Panjab University,  
Chandigarh 160 014, India

<sup>#</sup>Also at Jawaharlal Nehru Centre for Advanced Scientific Research,  
Bangalore 560 064, India

e-mail: dftqfd@pu.ac.in

**Abstract.** For the NO molecule, modelled as a Morse oscillator, time-dependent (TD) nuclear Schrödinger equation has been numerically solved for the multiphoton vibrational dynamics of the molecule under a far-infrared laser of wavelength 10503 nm, and four different intensities,  $I = 1 \times 10^8$ ,  $1 \times 10^{13}$ ,  $5 \times 10^{16}$ , and  $5 \times 10^{18}$  W cm<sup>-2</sup> respectively. Starting from the vibrational ground state at zero time, various TD quantities such as the norm, dissociation probability, potential energy curve and dipole moment are examined. Rich high-harmonics generation (HHG) spectra and above-threshold dissociation (ATD) spectra, due to the multiphoton interaction of vibrational motions with the laser field, and consequent elevation to the vibrational continuum, have been obtained and analysed.

**Keywords.** NO molecule; Morse oscillator; dissociation dynamics; vibrational HHG spectra; vibrational ATD spectra.

### **1. Introduction**

As a result of recent developments of femtosecond lasers of intensity up to about  $10^{18}$  W cm<sup>-2</sup>, there have been extensive experimental and theoretical research in order to obtain insights into multiphoton nonlinear interactions of atoms and molecules with intense laser fields.<sup>1-9</sup> A wealth of information now exists on such interactions. For atoms, major nonlinear phenomena include high-harmonics generation (HHG), above-threshold ionization (ATI), stabilization in superintense laser fields, etc. For molecules, apart from HHG and ATI, the dynamics of molecular dissociation (above-threshold dissociation) under intense laser fields can lead to ‘Coulomb explosion’ in which, as a result of ionisation, positively charged molecular fragments separate with increased speed.

For a diatomic molecule, if one does not explicitly consider interactions between electronic motions and intense laser fields (in other words, electronic motions only provide the potential in which nuclei move under Born–Oppenheimer approximation), the multiphoton interaction between vibrational motions and intense femtosecond far-IR lasers has not received adequate attention. Earlier studies were mainly concerned with

---

<sup>†</sup>Dedicated to Professor C N R Rao on his 70th birthday

\*For correspondence

excitation and dissociation dynamics starting from ground states of diatomic molecules, e.g. NO, HF and H<sub>2</sub> molecules under infrared and far-infrared lasers, usually of wavelengths 2468, 5250 and 5835 nm<sup>10-16</sup> and 166667 nm for excited states of I<sub>2</sub><sup>+17,18</sup> under intensities ranging from  $I = 10^{15} - 10^{16}$  W cm<sup>-2</sup>. There have also been studies on HHG on the ground state of HF molecule (both classical and quantum mechanical) with  $\lambda_L = 531$  nm<sup>19</sup> as well as on its excited states with  $\lambda_L = 193$  and 1074 nm with  $I = 3.5 \times 10^{15}$ ,  $3.5 \times 10^{17}$  and  $3.3 \times 10^{20}$  W cm<sup>-2</sup>.<sup>20</sup> Such HHG originated from multiphoton interactions between electrons and the laser fields. Most of these studies modelled the diatomic molecule as a Morse oscillator.

Against the above background, the objectives of the present theoretical study are the following.

- (1) Disregarding any explicit interactions between electrons and the laser fields, to study the dynamics of multiphoton interaction of the NO molecule, modelled as a Morse oscillator, with a far-infrared laser of wavelength  $\lambda_L = 10503.1241$  nm (such that two photons are necessary to excite the molecule from the ground vibrational to the first excited vibrational state and 68 photons are required to just lift the molecule from the ground state to the vibrational continuum) at four different intensities  $I = 1 \times 10^8$ ,  $1 \times 10^{13}$ ,  $5 \times 10^{16}$  and  $5 \times 10^{18}$  W cm<sup>-2</sup>. Note that in order to generate HHG and ATI from the He atom under an intense laser field of wavelength 1064 nm, 68 photons are necessary to just lift the He atom from its ground state to the electronic continuum. The choice of NO as a heteronuclear diatomic molecule for this study was made because NO is abundant in nature and living systems. It also appears to be one of the most studied molecules as far as its interactions within living bodies and with laser fields as well as its adsorption on solids are concerned.
- (2) To study time-dependent (TD) quantities such as probability density, dissociation probability, potential energy curve and dipole moment. Specifically, are the laser field and dipole moment in step?
- (3) To examine the possibility of an HHG spectrum arising from vibrational motions since this does not appear to have been studied for the molecule under such a low frequency.
- (4) To examine the vibrational above-threshold dissociation (ATD) or energy spectrum.
- (5) A comparison between the four different intensities.

Most of the results reported in this paper appear to be new and occasionally counter-intuitive.

The most accurate method for studying the dynamical evolution of quantum systems under strong driving forces is the numerical solution of the corresponding time-dependent Schrödinger equation (TDSE). In view of our earlier work on one-dimensional nonlinear oscillators under intense laser fields,<sup>21</sup> this is the method of calculation adopted in §2 below. Section 3 discusses the results while §4 makes a few concluding remarks.

## 2. Method of calculation

The one-dimensional Morse oscillator potential is

$$V(x) = D_e \exp[-\mathbf{a}(x - x_{eq})]^2, \quad (1)$$

where  $D_e$  is the dissociation energy,  $x$  is the internuclear distance,  $x_{eq}$  is the latter's equilibrium value (bond length) and  $\mathbf{a}$  is a positive constant.

The vibrational levels for this system under the Born–Oppenheimer approximation can be obtained by solving the nuclear Schrödinger equation involving the unperturbed Hamiltonian (atomic units employed throughout this paper),

$$H_0 = -\frac{1}{2\mathbf{m}d^2} + D_e \exp[-\mathbf{a}(x - x_{eq})]^2, \quad (2)$$

where  $\mathbf{m}$  is the reduced mass of the molecule. In the present work on the NO molecule, we have employed the following parameters.<sup>22</sup>

Morse frequency,  $\mathbf{w} = 1904.3 \text{ cm}^{-1} = 0.008676174 \text{ a.u.}$ ; anharmonicity constant,  $\mathbf{c} = 0.007336028$ ;  $D_e = 0.2957 \text{ a.u.}$ ;  $x_{eq} = 2.1747 \text{ a.u.}$ ;  $\mathbf{a} = 1.3209 \text{ a.u.}^{-1}$ ;  $\mathbf{m} = 13705.595 \text{ a.u.}$

There are 55 vibrational bound states associated with the unperturbed Hamiltonian in (2)<sup>16</sup>.

On applying the laser electric field, the Hamiltonian of the system becomes

$$H = H_0 + d(x) f(t) E_0 \sin(\mathbf{w}t), \quad (3)$$

where  $d(x)$  is the dipole moment operator (see (4) below),  $E_0$  is the maximum field strength ( $E_0 = \sqrt{8\mathbf{I}}/c$ ;  $\mathbf{I}$  is the laser intensity),  $\mathbf{w}$  is the incident laser frequency, and the ramp function  $f(t) = t/t_0$  up to three optical cycles ( $t_0 = 4345 \text{ a.u.} = 105.1 \text{ fs}$ ) and unity thereafter.

Ting<sup>12</sup> as well as Goggin and Milonni<sup>15</sup> employed  $d(x)$  as a linear function of internuclear distance. This definition has the problem of dipole moment increasing with  $x$  whereas it should actually decrease. To tackle this problem, we adopt Tanner and Maricq's<sup>17,18</sup> prescription of

$$d(x) = x \exp(-x/ax_{eq}), \quad (4)$$

where the value of ' $a$ ' was taken arbitrarily as 0.375. The same form was employed by Heather and Metiu<sup>10,11</sup> except that the exponent was different from that above and is the same for all diatomic molecules. They write

$$d(x) = x \exp(-Ax), \quad (5)$$

where  $A = 1.587 \text{ a.u.}$  In the present study of NO molecule, we have employed  $a = 0.2815$  in (4). For the ground state, this gives the expectation value of  $d(x)$  as 0.06247 a.u. compared to the experimental dipole moment, 0.06256 a.u.

The ground state wavefunction for the NO molecule is obtained by solving the TDSE,

$$H\Psi(x, t) = i \frac{\partial \Psi(x, t)}{\partial t}, \quad (6)$$

in imaginary time by first transforming the TDSE into a form resembling a diffusion quantum Monte Carlo (DQMC)-type equation.<sup>23</sup> The system is then evolved in imaginary time until a global minimum corresponding to the stationary ground state is reached (in real time, the ground state corresponds to  $t = 0$ ). The same procedure is to be followed to obtain the energy eigenvalues for excited states, maintaining the orthogonality of each state to all the lower states. The numerical methodology was reported earlier.<sup>24</sup> This

DQMC approach had successfully been employed earlier to obtain the energies of atomic and molecular systems<sup>25,26</sup> as well as those of double-well,<sup>24</sup> multiple-well<sup>27</sup> and self-interacting<sup>28</sup> nonlinear oscillators. Our calculated vibrational ground state energy for the NO molecule, neglecting rotational contributions and using  $\Delta x = 0.01$  (the same spatial mesh would be employed for real-time dynamics as given below), is  $\epsilon_0 = 0.004366$  a.u. compared to the analytical Morse eigenvalue  $\epsilon_0 = 0.004322$  a.u. However, it may be noted that using very fine spatial and temporal mesh as well as very low tolerance make the numerical method exact in principle.<sup>24</sup>

The dynamics of the vibrating NO molecule are then studied by employing the same algorithm for real time, thus solving the TDSE itself instead of a diffusion equation in real time. The system is allowed to evolve for 280 fs over 8 optical cycles under intense laser fields with a time step ( $\Delta t$ ) of 0.17680329 a.u. such that one optical cycle is completed in 8192 time steps. The incident laser frequency is chosen as  $\omega_L = 0.004338087$  a.u. which is exactly one-half of the calculated vibrational transition frequency between the ground state and the first excited state of the unperturbed Morse oscillator.

The other laser parameters are: wavelength,  $\lambda_L = 10503\text{-}1241$  nm; intensity,  $I = 1 \times 10^8$ ,  $1 \times 10^{13}$ ,  $5 \times 10^{16}$  and  $5 \times 10^{18}$  W cm<sup>-2</sup>; pulse length = 280 fs ( $\sim 11587$  a.u.).

In numerically solving the TDSE, (6), we have employed a large computation grid,  $0 \leq x \leq 980$  a.u., with the spacing  $\Delta x = 0.01$  a.u., i.e. 98000 space-grid points. The justification behind taking such a large grid is that the probability density for the system under the influence of a laser field is expected to spread rapidly and thereby encroach into the continuum. The use of a large computation grid obviates the necessity for using either an absorbing potential or a mask function.

### 3. Results and discussion

#### 3.1 Time-dependent probability density (norm)

We begin with the normalized ground state wavefunction of the system as the initial state at  $t = 0$ . The probability density (or, TD norm  $N(t) = \langle \Psi(x, t) | \Psi(x, t) \rangle$ ) plot for the same is nearly a Gaussian centred at  $x_{eq}$  (figure 1a). It is natural for the wavefunction to disperse as the system evolves in time. With the onset of the laser field, the wavefunction no longer remains like a simple Gaussian and begins to spread spatially like a wave packet. Initially, at  $t = 1.77$  a.u., this spread is less and several new peaks appear in the probability density, thereby revealing contributions from excited states (figure 1b). The presence of nodes and minima indicate the presence of pure excited states as well as superposition of states. As discussed in §3.2, probability density oozes out of the computation grid after the lapse of only  $\sim 9$  fs. At the end of the first optical cycle ( $t = 1448$ , a.u. = 35 fs), the probability density plot displays a very complicated accordion-like pattern of maxima (figure 1c), each maximum containing numerous peaks, spanning the whole grid even before the completion of ramp (at three optical cycles, figure 1d). Further time-evolution of the system leads to the participation of many more states such as higher excited states, dressed states and continuum states due to the large driving force of the laser field. Indeed, one should look for signatures of 'quantum chaos' in such a situation; however, this is not an objective of the present study. The probability density eventually leaks into the vibrational continuum with the creation of a final state that is dispersed over a large spatial region and has a reduced norm compared to the

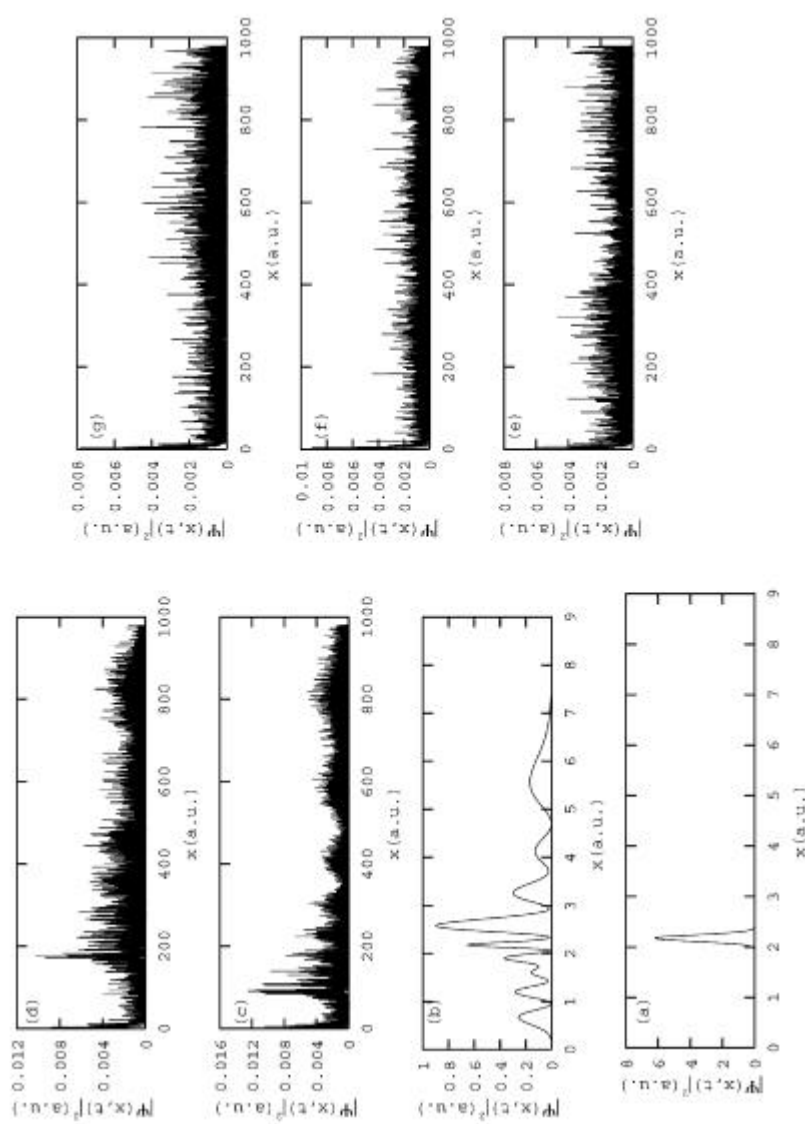


**Figure 1.** Probability density ( $|\Psi(x, t)|^2$ ) plots (a.u.) for  $I = 1 \times 10^8 \text{ W cm}^{-2}$  at (a) the start ( $t = 0$ ), (b) after 10 time-steps ( $t = 1.77 \text{ a.u.}$ ), (c) at the end of the first optical cycle ( $t = 1448 \text{ a.u.}$ ), (d) at the end of the third optical cycle ( $t = 4345 \text{ a.u.}$ ), (e) when the laser field  $E = E_0$  ( $t = 10501 \text{ a.u.}$ ), (f) when the laser field  $E = -E_0$  ( $t = 11225 \text{ a.u.}$ ), and (g) at the end of the eighth optical cycle ( $t = 11587 \text{ a.u.}$ ). Corresponding plots for  $I = 1 \times 10^{13} \text{ W cm}^{-2}$  are similar.

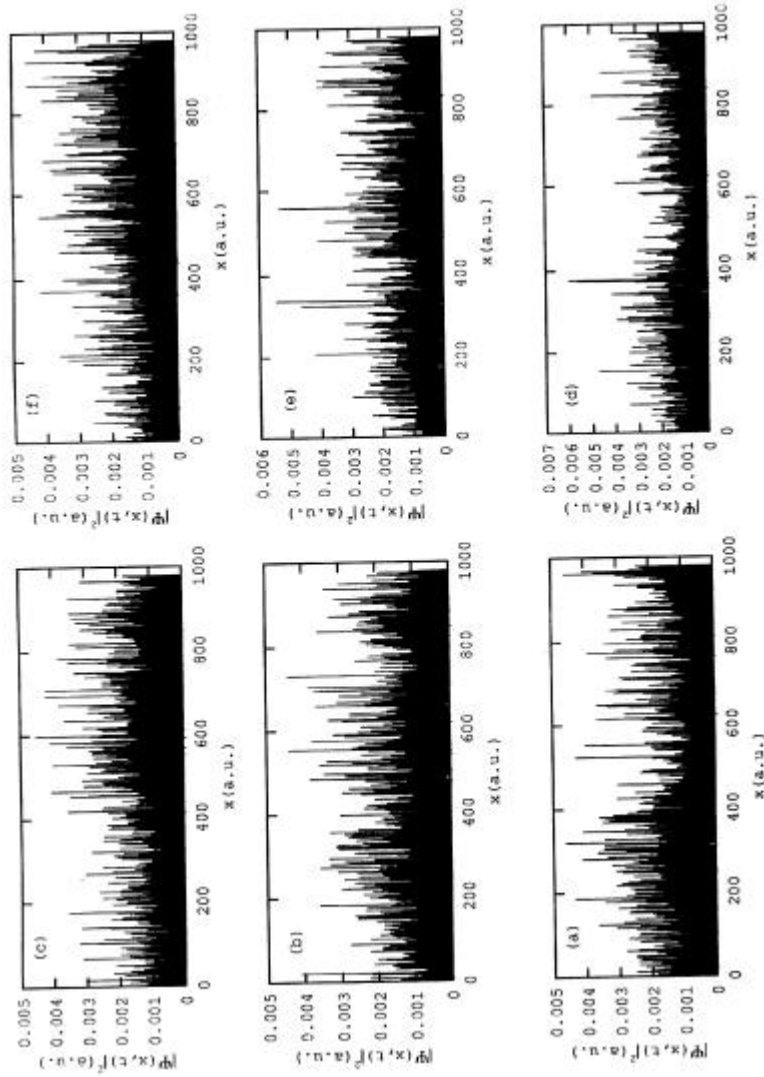


**Figure 2.** Probability density ( $|\Psi(x, t)|^2$ ) plots (a.u.) for  $I = 5 \times 10^{16} \text{ W cm}^{-2}$  at (a) when the laser field  $E = E_0$  ( $t = 10501$  a.u.), (b) when the laser field  $E = -E_0$  ( $t = 11225$  a.u.), (c) at the end of eighth optical cycle ( $t = 11587$  a.u.). Similar plots for  $I = 5 \times 10^{18} \text{ W cm}^{-2}$  at (d) when the laser field  $E = E_0$  ( $t = 10501$  a.u.), (e) when the laser field  $E = -E_0$  ( $t = 11225$  a.u.), and (f) at the end of 8th optical cycle ( $t = 11587$  a.u.). For both intensities, plots at  $t = 1-77, 1448, 4345$  a.u. are similar to those of figure 1b, c, d respectively.

initial norm of unity. This is evident in the probability density plots examined at the end of the ramp ( $t = 4345$ , a.u. = 105.1 fs), and at the eighth optical cycle when the laser field attains its maximum and minimum values,  $E = \pm E_0$  as well as zero (figures 1 and 2).

At the end of one optical cycle, the norm  $N(t)$  has already fallen from 1.0 to 0.8859 for all the four intensities, indicating  $\sim 11\%$  dissociation. Such a common value for all the four intensities, even though it concerns the initial stages of the interaction, is counter-intuitive. As time progresses, earlier larger peaks subside while the peaks near the grid-end increase in height indicating smaller proportions of ground and lower excited states in the complicated mixture that is the time-evolved wavefunction. For  $I = 5 \times 10^{16} \text{ W cm}^{-2}$  and  $5 \times 10^{18} \text{ W cm}^{-2}$ , peaks near the beginning, for the eighth optical cycle (figure 2), are smaller than those for  $I = 1 \times 10^8 \text{ W cm}^{-2}$  and  $1 \times 10^{13} \text{ W cm}^{-2}$ . All the peak heights fluctuate with time.

### 3.2 Time-dependent dissociation probability

In studying the dissociation dynamics of diatomic molecules under intense laser fields, several definitions for dissociation probability have been employed.<sup>10-12,17,18</sup> Here, in view of our deployment of a large spatial grid, we adopt the definition of the TD dissociation probability as<sup>13</sup>

$$P_{\text{diss}}(t) = 1 - N(t). \quad (7)$$

The definition is appropriate because with the probability density leaking into the continuum, through the computation grid, the norm  $N(t)$  decreases and this can be referred to as the onset of dissociation. Obviously, unless the probability density meanders outside the grid, the norm should remain unity. We have calculated  $P_{\text{diss}}(t)$  for the NO molecule under four different laser intensities. Interestingly, the final dissociation probability as well as its general variation (figure 3) is practically the same for all the intensities, indicating that this insensitivity to laser intensity is due to the threshold intensity for NO dissociation lying below  $I = 1 \times 10^8 \text{ W cm}^{-2}$ . In other words, even  $I = 1 \times 10^8 \text{ W cm}^{-2}$  is

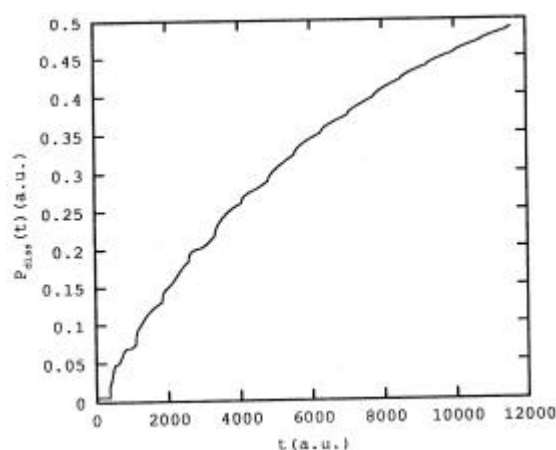


**Figure 3.** Dissociation probability,  $P_{\text{diss}}(t)$  vs  $t$  in a.u. for  $I = 1 \times 10^8 \text{ W cm}^{-2}$ . Plots for the other three intensities overlap on this plot although the values are not identical.

an intense laser for the present work. After an 'induction period' of  $t \cong 368$  a.u. ( $\sim 9$  fs), there is a rapid increase in  $P_{\text{diss}}(t)$ , followed by a gradual tapering off in the increase of  $P_{\text{diss}}(t)$  with time. Such behaviour is qualitatively similar to that observed by other workers.<sup>10-12,17,18</sup> For all the four intensities, about 50% dissociation is achieved at the completion of eight optical cycles. At the crest ( $E = E_0$ ) of the eighth optical cycle, the TD potential (see below),  $U(x, t)$ , reaches a constant value, 0.295685528 at  $x = 18.16$  a.u. for  $I = 1 \times 10^8$ ,  $1 \times 10^{13}$  and  $5 \times 10^{16}$   $\text{W cm}^{-2}$ , and at  $x = 18.11$  a.u. for  $I = 5 \times 10^{18}$   $\text{W cm}^{-2}$  (see the potential plot, figure 4). It is thus obvious that one must interpret the probability density spreading beyond  $x = 18.16$  a.u. as its gradual excursion into the continuum.

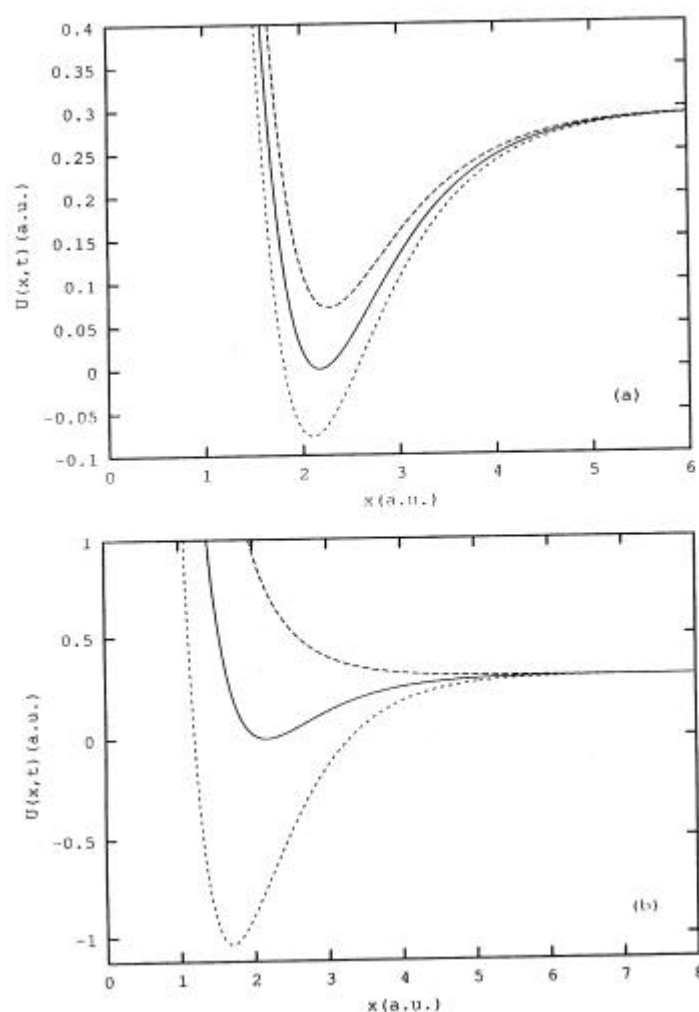


**Figure 4.** Time-dependent potential  $U(x, t)$  plots (a.u.) for (a)  $I = 5 \times 10^{16}$   $\text{W cm}^{-2}$  and (b)  $I = 5 \times 10^{18}$   $\text{W cm}^{-2}$ . The solid line refers to the unperturbed Morse potential, the dotted line above the Morse potential refers to the crest ( $E = E_0$ ) and the dotted line below the Morse potential refers to the trough ( $E = -E_0$ ) at the eighth optical cycle.

### 3.3 Time-dependent potential

The TD potential for the present problem is given by

$$U(x, t) = V(x) + d(x) f(t) E_0 \sin(\mathbf{w}t). \quad (8)$$

This TD potential reduces to the unperturbed Morse potential  $V(x)$  at  $t=0$  or when  $\sin(\mathbf{w}t)=0$ . At all other times,  $U(x, t)$  is modified by the strength of the laser field. Here, we examine the TD potential plots at  $t=0$ , as well as at times when the laser field attains its maximum and minimum values,  $E = \pm E_0$ , after seven optical cycles. The  $E_0$  values for different laser intensities are as follows.

$I(\text{W cm}^{-2})$	$1 \times 10^8$	$1 \times 10^{13}$	$5 \times 10^{16}$	$5 \times 10^{18}$
$E_0 \times 10^5$ (a.u.)	5.33794738	1688.00717	119360.132	1193601.32

An analysis of the potential  $U(x, t)$  plotted against time (figure 4) shows that it has the same appearance as the unperturbed Morse potential but with different well-depths. For all the cases, the well depth must decrease when  $E = +E_0$  and increase when  $E = -E_0$ . This change in well-depth is dependent on the strength of the laser field, and is quite small for  $I = 1 \times 10^8$  and  $1 \times 10^{13} \text{ W cm}^{-2}$ . However, for  $I = 5 \times 10^{16}$  and  $5 \times 10^{18} \text{ W cm}^{-2}$ , this change is significant (figure 4). For  $I = 5 \times 10^{18} \text{ W cm}^{-2}$ , the potential well disappears when  $E = E_0$ , leading to a repulsive potential which increases the rate of dissociation. However, this is partly compensated by a deep minimum at  $E = -E_0$ . Note that, for  $I = 5 \times 10^{16} \text{ W cm}^{-2}$ , the potential minimum shifts to left or right by about 1%. It has been argued before<sup>21</sup> that selection rules for transitions which are traditionally based on TD perturbation theory and do not explicitly consider the time-dependence of the potential are not applicable in cases like the present system where the TD potential can undergo drastic changes in shape.

### 3.4 High harmonics generation (HHG)

High harmonics generation is a consequence of the distribution of dipole moment induced by the laser electric field. The quantum mechanical dipole moment  $d(t)$  can be written as

$$d(t) = \langle \Psi(x, t) | d(x) | \Psi(x, t) \rangle, \quad (9)$$

where  $d(x)$  is the dipole moment operator (see (4)).

When the laser field is switched on, the dipole moment shows an initial maximum at  $t \cong 1$  a.u., followed by a sharp decrease and then, after crossing the ramp, settles down into a very complicated pattern with an oscillating envelope whose periodicity is twice that of the laser field (figure 5). Thus, for all the intensities employed in the present work, the net dipole moment is not in resonance with the field. The low values of dipole moment also point towards the system approaching dissociation. A comparison of dipole moments for all the four intensities and from  $t = 6000$ – $11587$  a.u. gives a counter-intuitive picture. The dipole moment plots for  $I = 1 \times 10^8$  and  $1 \times 10^{13} \text{ W cm}^{-2}$  appear nearly the same and so do the plots for  $5 \times 10^{16}$  and  $5 \times 10^{18} \text{ W cm}^{-2}$ . However, the former pair is different from the latter pair in that the time-average ( $t = 6000$ – $11587$  a.u.) dipole moments for, e.g.  $I = 1 \times 10^{13}$  and  $5 \times 10^{18} \text{ W cm}^{-2}$  are  $3.630 \times 10^{-4}$  and  $1.534 \times 10^{-4}$  a.u. respectively. Consequently, the HHG peaks for the latter intensity are

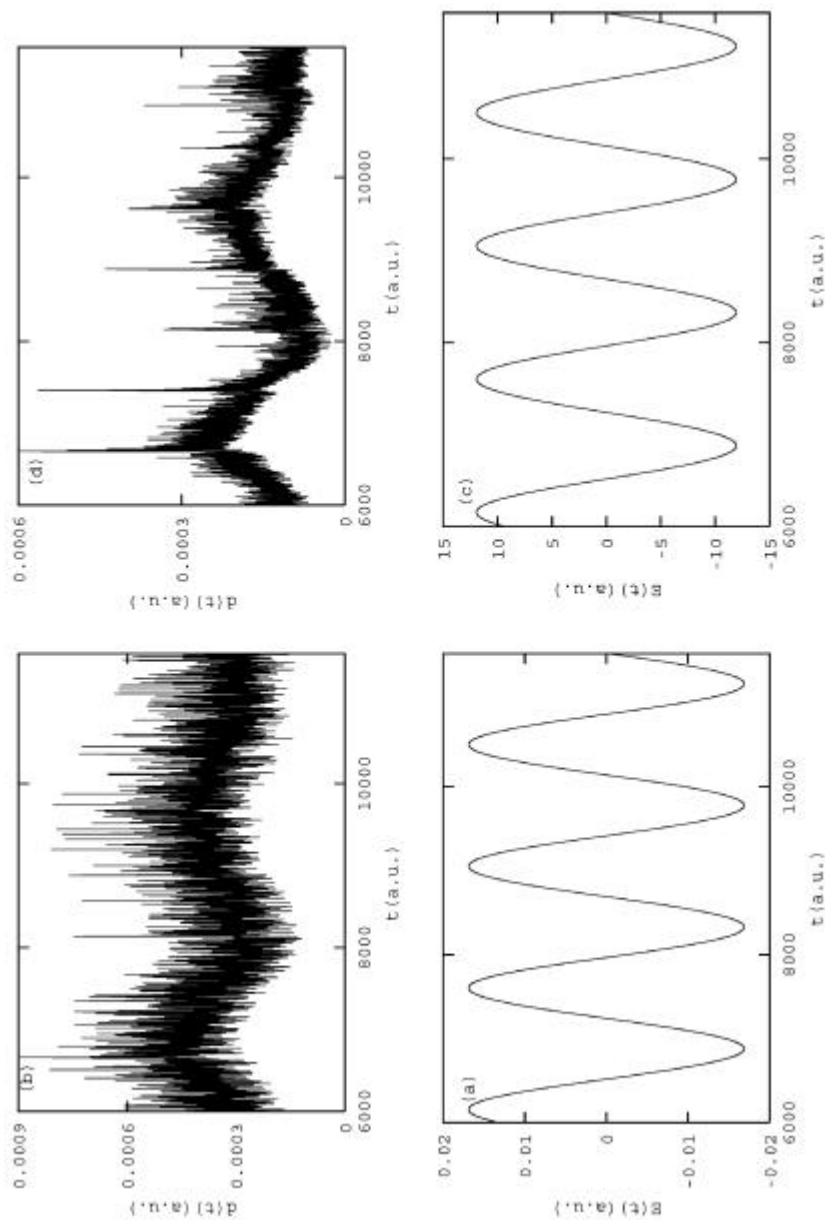


**Figure 5.** Dipole moment  $d(t)$  and laser electric field vs  $t$  in a.u. from  $t = 6000$ – $11587$  a.u. (a) Field corresponding to  $I = 1 \times 10^{13} \text{ W cm}^{-2}$ , (b)  $d(t)$  for  $I = 1 \times 10^{13} \text{ W cm}^{-2}$ , (c) field corresponding to  $I = 5 \times 10^{18} \text{ W cm}^{-2}$ , (d)  $d(t)$  for  $I = 5 \times 10^{18} \text{ W cm}^{-2}$ .

generally lower in height by approximately a factor of two, compared to those for the former intensity (see below). As mentioned before, the interaction of electrons with the laser is not being considered in the present work and thus the time-evolving dipole moment mentioned is not electronic in origin. Had it been so, the dipole moment would have been more effective in the generation of harmonics. Nevertheless, the present TD dipole moment is not quite negligible and therefore HHG is expected. In order to probe this phenomenon, a fast Fourier transform (FFT) of  $d(t)$  is performed over the last four optical cycles with integration limits  $t_1 = 5793.5$  a.u. and  $t_2 = 11587$  a.u. as

$$|D(\omega)|^2 = \left| \int_{t_1}^{t_2} d(t) e^{-i\omega t} dt \right|^2 ; \quad d(-t) = d(t). \quad (10)$$

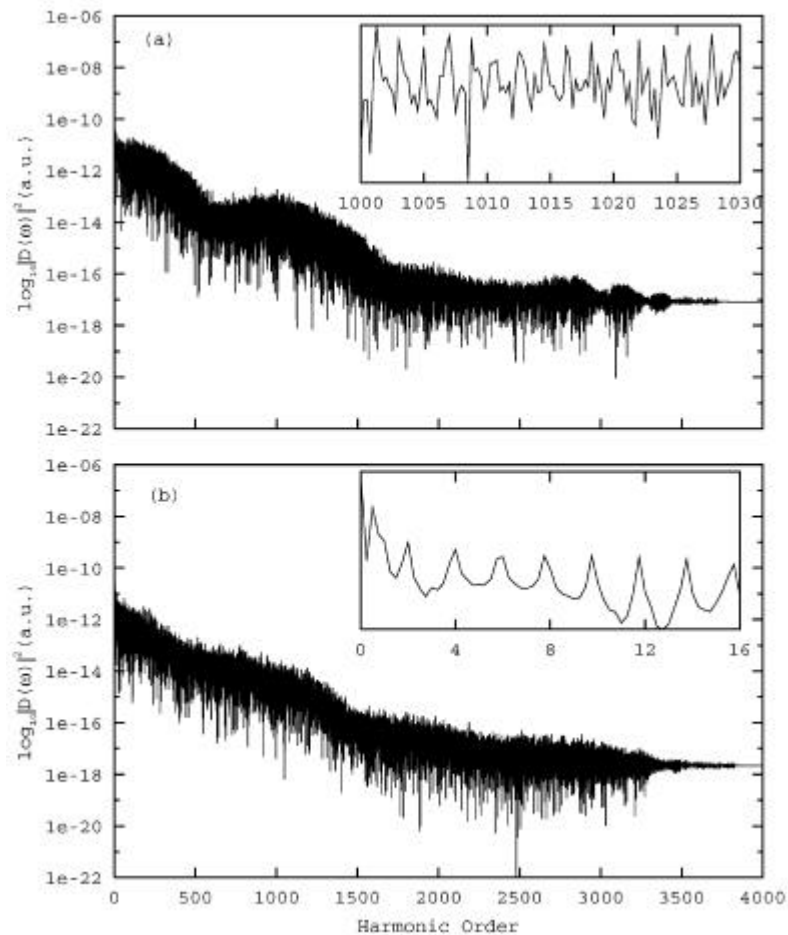


**Figure 6.** Vibrational HHG spectra (a.u.) obtained by plotting  $\log_{10}|D(\omega)|^2$  (a.u.) against harmonic order ( $\omega/\omega_L$ ) at laser intensities (a)  $1 \times 10^8 \text{ W cm}^{-2}$  and (b)  $5 \times 10^{18} \text{ W cm}^{-2}$ . Inset of (a) shows odd, even and shifted harmonics, while inset of (b) shows the first few prominent even harmonics. Plots for  $I = 1 \times 10^{13}$  and  $5 \times 10^{16} \text{ W cm}^{-2}$  are similar to those of (a) and (b) respectively.

A plot of  $|D(\mathbf{w})|^2$  vs harmonic order displays a spectrum (figure 6) with the same characteristic features as those of the atomic and molecular HHG spectra, viz. a rapid decay of peak intensities for the first few harmonics, followed by a plateau of harmonics with nearly the same intensities and then a sharp cut-off. For real systems, there is a characteristic threshold intensity below which no significant harmonic generation is observed. Above this threshold, harmonics begin to appear with an appreciable increase in the number of peaks and an extension of the plateau at high intensities. However, the HHG spectra analysed for different intensities in the present work do not show marked differences in their features. The spectra are actually very rich in peaks, indicating that up to about 3500 multiples of incident laser frequency are being produced, although the peaks are of low intensity as a consequence of low dipole moments induced by the laser field. The first harmonic is present as a discernible kink and there is a relatively most intense low-frequency peak at harmonic order 0.5 (figure 6). This is true for all  $I > 10^{13} \text{ W cm}^{-2}$  employed in the present case. Such low-frequency peaks were earlier observed and interpreted for nonlinear oscillators.<sup>21</sup> However, at  $I = 1 \times 10^8 \text{ W cm}^{-2}$ , while the low-frequency component is present, the first harmonic has disappeared. Interestingly, the beginning of the HHG spectra for all the four laser intensities shows sharp even harmonics and absence of odd harmonics (except the first harmonic when  $I > 10^{13} \text{ W cm}^{-2}$ ) but thereafter odd harmonics also appear and the spectrum is dense with odd, even and shifted harmonics. Such a phenomenon has also been observed earlier for HHG spectra produced by nonlinear oscillators.<sup>21</sup> The appearance of both odd and even harmonics is due to the fact that the Morse potential is neither symmetric nor antisymmetric. In all the cases, the HHG shows a 'staircase' spectrum with six distinct bumps indicating that the first bump is associated with the ground state while the last bump is associated with the fifth excited state. The successive appearance of lower and lower plateaus indicates significant dissociation; the peaks in the plateau region are of low intensity but should not be neglected. This simultaneous occurrence of harmonic generation and dissociation is an interesting observation. It is also clear that transitions occur from continuum high energy levels to lower ones.

The emergence of a 'staircase' HHG spectrum was first reported recently<sup>21</sup> in the case of one-dimensional nonlinear oscillators with either pseudodegenerate energy levels or low-lying excited states. However, so far such a spectrum has not been detected experimentally. For the NO molecule, quite apart from a 'staircase' HHG spectrum originating from vibrational energy levels, such a spectrum should also originate from electronic energy levels because NO has a doubly degenerate ground electronic state and a low-lying doubly degenerate excited state. Indeed, 'staircase' HHG spectra may be encountered more frequently than one might have anticipated.

The above harmonics generation arising from the contributions of only vibrational states does not seem to have been studied before, presumably due to the less intense HHG compared to that obtained from interaction of lasers with electronic motion. The harmonics obtained in the present work need to be enhanced in order to exploit them for practical purposes. One way to achieve it would be to realize phase-matching of identical harmonics generated by an assembly of NO molecules in the gas phase.

### 3.5 Vibrational ATD (energy) spectrum

An interaction with intense lasers modifies the internal structure of a system because the applied electric field is a large perturbation comparable to the internal fields of the

system. Atoms and molecules placed in such intense fields tend to ionise and can even absorb more than the minimum number of photons required for ionisation thus exhibiting the interesting nonlinear phenomenon of above-threshold ionisation (ATI). Molecules, possessing multiple charge centres, show additional degrees of freedom for decay via dissociation. This can be followed by absorption of more than the minimum number of photons required for dissociation (above-threshold dissociation (ATD)). In molecules, ATI is the precursor of ATD; in other words, molecular dissociation follows ionisation *after* the molecule has been raised to the *electronic* continuum. In the present work, ATD refers strictly to the *vibrational* continuum and is therefore analogous to ATI in atoms. A characteristic ATI spectrum from atoms or ATI-like spectrum from nonlinear oscillators<sup>21</sup> shows neighbouring peaks separated by exactly the photon energy ( $\omega$  in a.u.). As discussed below, an identical situation is encountered with the vibrational ATD. The ATD spectra are obtained by calculating the FFT,  $A(\omega)$  of the autocorrelation function  $C(t)$  for the last four optical cycles with integration limits  $t_1 = 5793.5$  a.u. and  $t_2 = 11587$  a.u. and plotting its modulus square vs the frequency components,

$$C(t) = \langle \Psi(x, t) | \Psi(x, 0) \rangle; C(-t) = C(t)$$

$$|A(\omega)|^2 = \left| \int_{t_1}^{t_2} C(t) e^{-i\omega t} dt \right|^2. \quad (11)$$

ATD spectra for  $I = 1 \times 10^8$  and  $1 \times 10^{13} \text{ W cm}^{-2}$  (figure 7a, b) show the presence of a single prominent peak of height  $1.4 \times 10^{-4}$  just before  $\omega = 0.29$  a.u. This is near the dissociation limit. In the ATD spectrum of  $I = 5 \times 10^{16} \text{ W cm}^{-2}$  (figure 7c inset), we observe a few prominent peaks separated by the photon energy in the range  $\omega = 0.265 - 0.32$  a.u., the three largest peaks being at  $\omega = 0.292, 0.283$  and  $0.279$  a.u. respectively. The ATD spectra for all the above three intensities reveal that these prominent peaks are followed by six bumps or packets of wriggles having low magnitudes of  $\sim 10^{-8}$  (as compared to  $10^{-4}$  of the highest peak for  $I = 1 \times 10^8$  and  $1 \times 10^{13} \text{ W cm}^{-2}$ , and  $10^{-6}$  of the highest peaks for  $I = 5 \times 10^{16} \text{ W cm}^{-2}$ ). These wriggles are not spaced by incident laser frequency, are continuous and may be attributed to the higher continuum states coming into the picture. Note that six bumps were earlier observed for HHG spectra (see above). The ATD energy spectrum at  $I = 5 \times 10^{18} \text{ W cm}^{-2}$  shows a rich spectrum (figure 7d) consisting of numerous peaks some of which appear to be multiplets and the six bumps are again clearly observable here. Plotted on the same scale as for  $I = 1 \times 10^8$  and  $1 \times 10^{13} \text{ W cm}^{-2}$ , the ATD spectral peak heights for  $I = 5 \times 10^{18} \text{ W cm}^{-2}$  are hardly discernible. To the best of our knowledge, such vibrational ATD spectra (without ATI) may not have been observed before.

#### 4. Conclusion

One-dimensional nonlinear oscillators are counter-intuitive and full of surprises. In both static and dynamic situations, they are a rich source of knowledge and understanding. Among them, the Morse oscillator stands in a class of its own. In the present work on the vibrational dynamics of NO molecule, modelled as a Morse oscillator, under intense laser fields of wavelength 10,503 nm, the following additional information and insights have been obtained; these supplement earlier works on the same system, which employed much smaller laser wavelengths.

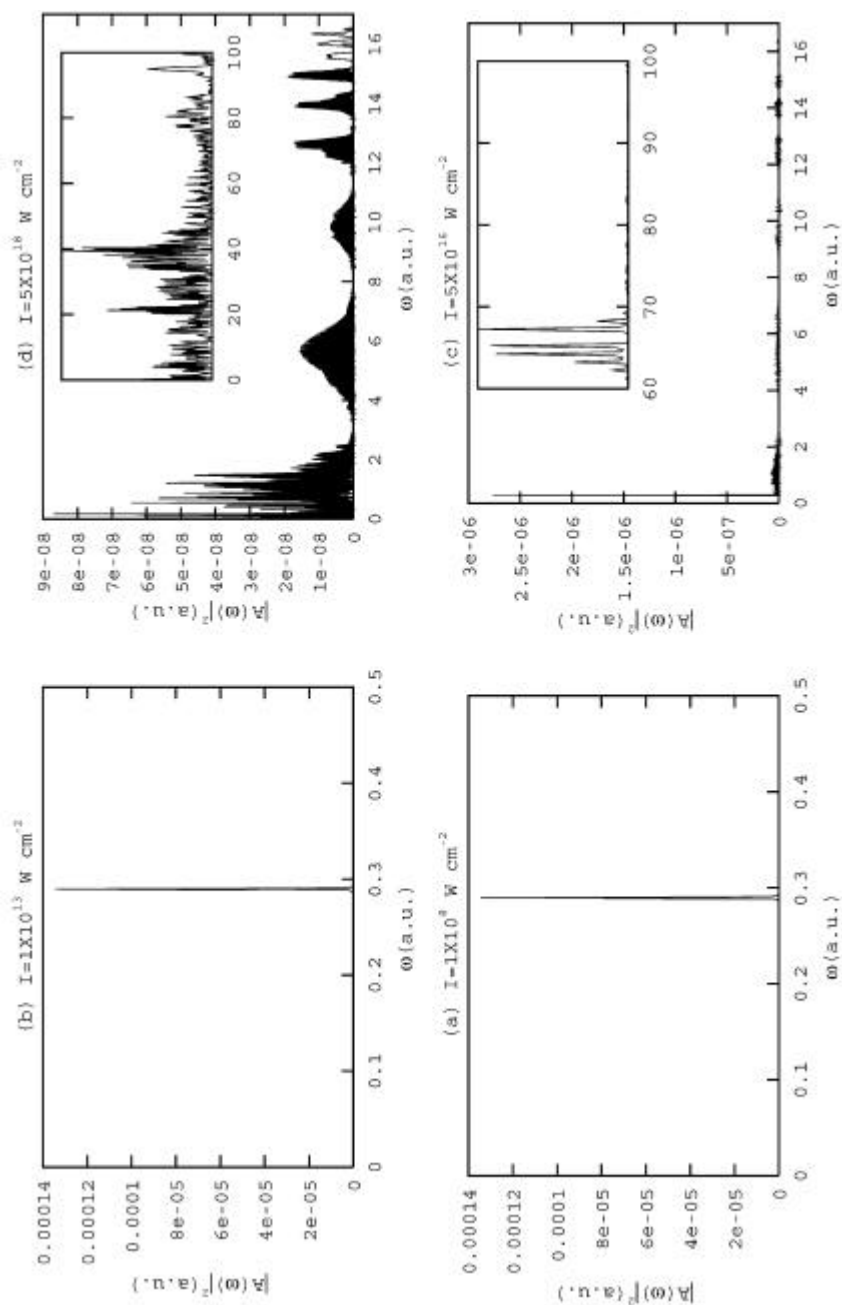


**Figure 7.** Vibrational ATD (energy) spectra obtained by plotting  $|A(\omega)|^2$  (a.u.) against frequency  $\omega$ , in a.u., at laser intensities (a)  $1 \times 10^8 \text{ W cm}^{-2}$ , (b)  $1 \times 10^{13} \text{ W cm}^{-2}$ , (c)  $5 \times 10^{15} \text{ W cm}^{-2}$  and (d)  $5 \times 10^{18} \text{ W cm}^{-2}$ . Inset of (c) shows prominent peaks vs harmonic order 60–100 whereas inset of (d) shows peaks vs harmonic order 0–100.

- (1) After about 9 fs, the probability density makes significant excursion into the vibrational continuum and the molecule begins to dissociate rapidly. Up to 280 fs, there is nearly 50% dissociation.
- (2) After the ramp has been reached, the periodicity in the dipole moment is twice that of the laser electric field.
- (3) Depending on the laser intensity (wavelength kept constant), the TD potential energy curve undergoes *interesting changes in shape from time to time*, except when  $\sin(\mathbf{w}t) = 0$ . Such changes include lowering and increasing the depth of the potential minimum, modifying the attractive potential into a repulsive potential and so on. Therefore, selection rules for spectral transitions which are usually based on TD perturbation theory would not be applicable in such a situation where traditional perturbation theory is not valid.
- (4) The vibrational HHG spectrum, which is an outcome of the system in the ground state being excited deep inside the vibrational continuum by the absorption of *many* photons, is rich in harmonics up to the 3500th harmonic (note that only 68 photons are needed to just reach the continuum from the ground state). These odd, even and shifted harmonics arise strictly due to vibrational states and do not seem to have been observed before. There is also a low-frequency component below the first harmonic. The six bumps in the 'staircase' HHG spectrum are identified as originating from the ground and first five vibrationally excited states. It appears that the 'staircase' HHG spectrum (see also ref. [21]) is waiting to be discovered experimentally! The relatively low intensities of the harmonics may be augmented by phase-matching of identical emissions from different NO molecules in the gas phase.
- (5) The vibrational ATD spectrum (energy spectrum), which is also an outcome of the molecule being lifted deep inside the vibrational continuum, is somewhat analogous to an atomic ATI spectrum. If the laser intensity is sufficiently high ( $5 \times 10^{16} \text{ W cm}^{-2}$  in the present case), the ATD spectrum shows peaks separated by exactly the photon energy. At a higher intensity, there are numerous multiplets of peaks. Like the HHG spectrum, the ATD spectrum also shows six bumps.

### Acknowledgement

The authors thank the Council of Scientific & Industrial Research, New Delhi, for financial support.

### References

1. Gavrilu M (ed.) 1992 *Atoms in intense laser fields* (New York: Academic Press)
2. Mittleman M H 1993 *Introduction to the theory of laser-atom interactions* (New York: Plenum)
3. Faisal F H M 1987 *Theory of multiphoton processes* (New York: Plenum)
4. Bandrauk A D (ed.) 1994 *Molecules in laser fields* (New York: Marcel Dekker)
5. Burnett K, Reed V C and Knight P L 1993 *J. Phys.* **B26** 561
6. Protopapas M, Keitel C H and Knight P L 1997 *Rep. Prog. Phys.* **60** 389
7. Joachain C J, Dörr M and Kylstra N J 2000 *Adv. At. Mol. Opt. Phys.* **42** 225
8. Eberly J H, Grobe R, Law C K and Su Q 1992 *Adv. At. Mol. Opt. Phys. (Suppl.)* **1** 301
9. Eberly J H and Kulander K C 1993 *Science* **262** 1229
10. Heather R and Metiu H 1987 *J. Chem. Phys.* **86** 5009
11. Heather R and Metiu H 1988 *J. Chem. Phys.* **88** 5496
12. Ting J J-L 1994 *J. Phys.* **B27** 1249
13. Ting J J-L 1995 *Phys. Rev.* **A51** 2641

14. Walker R B and Preston R K 1977 *J. Chem. Phys.* **67** 2017
15. Goggin M E and Milonni P W 1988 *Phys. Rev.* **A37** 796
16. Lin J T, Hayashi M, Lin S H and Jiang T F 1999 *Phys. Rev.* **A60** 3911
17. Tanner J J and Maricq M M 1988 *Chem. Phys. Lett.* **149** 503
18. Tanner J J and Maricq M M 1989 *Phys. Rev.* **A40** 4054
19. Averbukh V and Moiseyev N 1998 *Phys. Rev.* **A57** 1345
20. Jiang T F 1993 *Phys. Rev.* **A48** 3995
21. Wadehra A, Vikas and Deb B M 2003 *J. Chem. Phys.* **119** 6620
22. Berry R S, Rice S A and Ross J 2000 *Physical chemistry* (Oxford: University Press) p. 189
23. Hammond B L, Lester W A Jr and Reynolds P J 1994 *Monte Carlo methods in ab initio quantum chemistry* (Singapore: World Scientific)
24. Roy A K, Gupta N and Deb B M 2002 *Phys. Rev.* **A65** 012109
25. Dey B K and Deb B M 1999 *J. Chem. Phys.* **110** 6229
26. Roy A K, Dey B K and Deb B M 1999 *Chem. Phys. Lett.* **308** 523
27. Gupta N, Roy A K and Deb B M 2002 *Pramana – J. Phys.* **59** 575
28. Wadehra A, Roy A K and Deb B M 2003 *Int. J. Quantum Chem.* **91** 597